Arts & Sciences Articles

Arts and Sciences

2015

Imaginary time density-density correlations for two-dimensional electron gases at high density

M. Motta

D. E. Galli

S. Moroni

E. Vitali
William & Mary

Imaginary time density-density correlations for two-dimensional electron gases at high density

M. Motta, D. E. Galli, S. Moroni, and E. Vitali

View Online   Export Citation   CrossMark

ARTICLES YOU MAY BE INTERESTED IN

The Journal of Chemical Physics

The Emerging Investigators Special Collection and Awards
Recognizing the excellent work of early career researchers!

Submit Today

Imaginary time density-density correlations for two-dimensional electron gases at high density

M. Motta,[1] D. E. Galli,[1] S. Moroni,[2] and E. Vitali[3]

[1]*Dipartimento di Fisica, Università degli Studi di Milano, Via Celoria 16, 20133 Milano, Italy*
[2]*IOM-CNR DEMOCRITOS National Simulation Center and SISSA, Via Bonomea 265, 34136 Trieste, Italy*
[3]*Department of Physics, College of William and Mary, Williamsburg, Virginia 23187-8795, USA*

We evaluate imaginary time density-density correlation functions for two-dimensional homogeneous electron gases of up to 42 particles in the continuum using the phaseless auxiliary field quantum Monte Carlo method. We use periodic boundary conditions and up to 300 plane waves as basis set elements. We show that such methodology, once equipped with suitable numerical stabilization techniques necessary to deal with exponentials, products, and inversions of large matrices, gives access to the calculation of imaginary time correlation functions for medium-sized systems. We discuss the numerical stabilization techniques and the computational complexity of the methodology and we present the limitations related to the size of the systems on a quantitative basis. We perform the inverse Laplace transform of the obtained density-density correlation functions, assessing the ability of the phaseless auxiliary field quantum Monte Carlo method to evaluate dynamical properties of medium-sized homogeneous fermion systems. © *2015 AIP Publishing LLC*. [http://dx.doi.org/10.1063/1.4934666]

I. INTRODUCTION

The homogeneous electron gas (HEG) is one of the most widely studied systems in condensed matter Physics.[1–6] It represents a model of recognized importance, which offers the opportunity to explore the quantum behavior of many-body systems on a fundamental basis and provides a ground test for several quantum chemistry,[7] many-body,[8] and quantum Monte Carlo (QMC)[4,9–11] methodologies. Furthermore, recent years have witnessed the realization of increasingly high-quality two-dimensional (2D) HEGs in devices of considerable experimental interest such as quantum-well structures[12,13] and field-effect transistors.[14]

The accuracy of QMC calculations for the HEG is unavoidably limited by the well-known sign problem,[15,16] arising from the antisymmetry of many-fermion wavefunctions. The vast majority of QMC simulations of many-fermion systems circumvent the sign problem relying on the Fixed-Node (FN) approximation.[17,18] Methodologies based on the FN approximation provide very accurate estimations of ground state properties such as the kinetic and potential energies, and the static structure factor. On the other hand, as the extension of the FN approximation to the manifold of excited states is less understood and established,[19,20] the study of dynamical properties of many-fermion systems is a very active and challenging research field.[19,21–26]

In a recent work,[19] performing an extensive study of exactly solvable few-fermion Hamiltonians, we have shown that the phaseless auxiliary field Quantum Monte Carlo (AFQMC)[22,27–36] method (the term phaseless denotes the approximation with which the method mitigates the sign problem) provides accurate estimates of imaginary time correlation functions (ITCFs) for few-fermion systems.

This encouraging results, however, do not grant that the methodology is able to provide accurate quantitative results for larger systems. In this paper, we apply the phaseless AFQMC to the calculation of ITCFs for much larger systems. We evaluate density-density correlation functions $F(\boldsymbol{q}, \tau)$ for two-dimensional homogeneous electron gases of up to 42 particles and we perform their inverse Laplace transform to extract information about the excitations of the system. We finally assess the accuracy of the calculations comparing AFQMC results with predictions within the random phase approximation (RPA) for finite systems.[8,37] We also compare AFQMC estimates with the results of FN calculations,[11,38] performed with a nodal structure encompassing optimized backflow correlations.[10,39,40]

The calculation of ITCFs is more difficult than the calculation of ground-state properties since, in the long imaginary time limit, the estimates of ITCFs are affected by a form of numerical instability that becomes more and more severe as the number of particles is increased. We face this issue using a stabilization technique, that was not necessary for the few-fermions systems,[19] for improving the quality of our estimates of ITCFs.

The unavoidable restrictions of the determinantal methodology (to study finite systems and to work with a finite basis set in the one-particle Hilbert space) and the difficulties related to the stabilization of ITCFs provide some limitations. In the particular case of the electron gas, the severity of such limitations increases with the Seitz radius r_s.[5] First, increasing r_s, the number of plane waves required to reach convergence in the basis set size becomes larger. Moreover, as detailed below, density-density ITCFs decay in a typical time τ which increases at least as $r_s^{3/2}$. This makes more and more demanding the task of extracting physical information on a quantitative

basis. Therefore, we focus on the high-density regime, which is nevertheless extremely interesting as the presence of the interaction leads to the emergence of important correlation effects, enhanced by the low dimensionality.

The paper is organized as follows: the phaseless AFQMC method is briefly reviewed in Section II, the results of the study are discussed in Section III, and conclusions are drawn in Section IV.

II. METHODOLOGY

A. The model

The 2D HEG is a system of charged spin-$\frac{1}{2}$ fermions interacting with the Coulomb potential and immersed in a uniform positively charged background. For the purpose of studying the 2D HEG, we simulate a system of N particles moving inside a square region $\mathcal{R}$ of surface $\Omega = L^2$, employing periodic boundary conditions (PBC) at the boundaries of the simulation domain, in conjunction with an Ewald summation procedure.[41] In the present work, energies are measured in Hartree units E_{Ha}, and lengths in Bohr radii a_B. The Hamiltonian of the system reads, in such units,

$$\hat{H} = \sum_{k\sigma} \frac{|k|^2}{2} \hat{a}^\dagger_{k\sigma} \hat{a}_{k\sigma} + \frac{1}{2\Omega} \sum_{q\neq 0} \frac{2\pi}{|q|} \sum_{\substack{k\sigma \\ p\varsigma}} \hat{a}^\dagger_{k+q\sigma} \hat{a}^\dagger_{p-q\varsigma} \hat{a}_{p\varsigma} \hat{a}_{k\sigma}, \quad (1)$$

where spin-definite plane waves

$$\varphi_{k\sigma}(r,\omega) = \frac{e^{ik\cdot r}}{\sqrt{\Omega}} \delta_{\omega, \frac{1}{2}-\sigma} \quad \frac{L}{2\pi} k \in \mathbb{Z}^2, \ \sigma = \pm\frac{1}{2} \quad (2)$$

with $r \in \mathcal{R}$, $\omega = 0, 1$ are used as a basis for the single-particle Hilbert space. The ground-state energy per particle of the system is obtained adding, to the mean value of (1), the corrective constant term,

$$\xi = \frac{1}{2L} \left[2 \sum_{\substack{n \in \mathbb{Z}^2 \\ n\neq 0}} \frac{\mathrm{erfc}\left(\sqrt{\pi}|n|\right)}{|n|} - 4 \right] = -3.900\,265\,\frac{1}{2L} \quad (3)$$

arising from the Ewald summation procedure employed.[41] Hamiltonian (1) can be parametrized in terms of the dimensionless Seitz radius r_s defined by

$$\frac{\Omega}{N} = \frac{1}{n} = \pi r_s^2 a_B^2, \quad (4)$$

where n is the density of the system and a_B the Bohr radius. This parametrization shows that the matrix elements of the kinetic energy roughly scale as $|k|^2 \simeq r_s^{-2}$, and those of the potential energy as $1/\Omega|q| \simeq r_s^{-1}$. Thus, for increasing Seitz radius, the interaction part of $\hat{H}$ plays a more and more relevant role.

B. The phaseless AFQMC

To address the calculation of static and dynamical properties of the 2D HEG, we resort to the phaseless AFQMC method,[22,27–36] which relies on the observation that the imaginary time propagator $e^{-\tau\hat{H}}$ acts as a projector onto the ground state $|\Phi_0\rangle$ of the system in the limit of large imaginary time.

Therefore, as long as a trial state $|\Psi_T\rangle$ has non-zero overlap with $|\Phi_0\rangle$, the relation

$$|\Phi_0\rangle \propto \lim_{\tau\to\infty} e^{-\tau(\hat{H}-\epsilon_0)}|\Psi_T\rangle \quad (5)$$

holds, ϵ_0 being the ground state energy, that can be estimated adaptively following a common procedure in Diffusion Monte Carlo (DMC) calculations.[42] QMC methods rely on the observation that deterministic evolution (5) can be mapped onto suitable stochastic processes and solved by randomly sampling appropriate probability distributions. Determinantal QMC methods, such as the phaseless AFQMC, use a Slater determinant as trial state $|\Psi_T\rangle$, typically the Hartree-Fock state, and map (5) onto a stochastic process in the abstract manifold $\mathfrak{D}(N)$ of N-particle Slater determinants. This association is accomplished by a discretization of the imaginary time propagator $e^{-\tau(\hat{H}-\epsilon_0)}$,

$$e^{-\tau(\hat{H}-\epsilon_0)}|\Psi_T\rangle = \left(e^{-\delta\tau(\hat{H}-\epsilon_0)} \right)^n |\Psi_T\rangle \quad n \in \mathbb{N}, \delta\tau = \frac{\tau}{n} \quad (6)$$

and by a combined use of the Trotter-Suzuki decomposition,[43,44] of the transformation[31,45,46] and of an importance sampling technique[19,31] on the propagator $e^{-\delta\tau(\hat{H}-\epsilon_0)}$. The result is

$$e^{-\delta\tau(\hat{H}-\epsilon_0)}|\Psi_T\rangle \simeq \int dg(\eta) \, \mathfrak{W}[\eta, \xi] \, \frac{\hat{G}(\eta-\xi)|\Psi_T\rangle}{\langle\Psi_T|\hat{G}(\eta-\xi)|\Psi_T\rangle},$$

where $dg(\eta)$ is a multidimensional standard normal probability distribution, $\hat{G}(\eta)$ is a product of exponentials of one-body operators, and

$$\mathfrak{W}[\eta, \xi] = e^{-\frac{\xi\cdot\xi}{2}-\eta\cdot\xi}\langle\Psi_T|\hat{G}(\eta-\xi)|\Psi_T\rangle \quad (7)$$

is a weight function depending on a complex-valued parameter ξ, which is chosen to minimize fluctuations in $\mathfrak{W}[\eta, \xi]$ to first order in $\delta\tau$. Equation (7) illustrates the mechanism responsible for the appearance of the sign problem in the framework of AFQMC: *when the overlap between $\hat{G}(\eta-\xi)|\Psi_T\rangle$ and the trial state vanishes* massive fluctuations occur in (7). In the method conceived by Zhang, the *exact* complex-valued weight function appearing in (7) is replaced[19,30] by the approximate form

$$\mathfrak{W}[\eta, \xi] \simeq e^{-\delta\tau(\epsilon_{loc}(\hat{G}(\eta-\xi)|\Psi_T))-\epsilon_0)} \times \max(0, \cos(\Delta\theta)), \quad (8)$$

where $\epsilon_{loc}(\Psi) = \mathrm{Re}\left[\frac{\langle\Psi_T|\hat{H}|\Psi\rangle}{\langle\Psi_T|\Psi\rangle} \right]$ is the *local energy* functional, and

$$\Delta\theta = \mathrm{Im}\left[\log\left[\frac{\langle\Psi_T|\hat{G}(\eta-\xi)|\Psi\rangle}{\langle\Psi_T|\Psi\rangle} \right] \right]. \quad (9)$$

The first factor corresponds to the *real local energy approximation*, which turns (7) into a *real quantity*, avoiding phase problems rising from complex weights; the real local energy approximation is implemented neglecting some fluctuations in the auxiliary fields.[19] The second factor, together with the introduction of the shift parameters, has been argued in Refs. 30 and 31 to keep the overlap between the determinants involved in the random walk and the trial determinant far from zero. In fact, the angle $\Delta\theta$ corresponds to the flip in the phase of a determinant during a step of the random walk: the term $\max(0, \cos(\Delta\theta))$ is meant to suppress determinants whose

phase undergoes an abrupt change, under the assumption[30,31] that such behaviour indicates the vanishing of the overlap with the trial state.

C. Hubbard-Stratonovich transformation in the plane-wave basis set

In general, the structure of $\hat{G}(\boldsymbol{\eta})$ is specified through a procedure that might result lengthy and computationally expensive.[19,31] When spin-definite plane waves are used as a basis for the single-particle Hilbert space, a remarkable simplification derived in details in Appendix A occurs in its calculation and leads to the following result:

$$\hat{G}(\boldsymbol{\eta}) = e^{-\frac{\delta\tau}{2}\hat{H}_0} e^{-i\sqrt{\delta\tau}\sum_{q\neq 0}\eta_{1q}\hat{A}_1(q)+\eta_{2q}\hat{A}_2(q)} e^{-\frac{\delta\tau}{2}\hat{H}_0}, \quad (10)$$

with

$$\hat{H}_0 = \sum_{k\sigma}\left(\frac{|\boldsymbol{k}|^2}{2} - \frac{1}{2\Omega}\sum_{p\neq k}\frac{2\pi}{|\boldsymbol{p}-\boldsymbol{k}|}\right)\hat{a}^\dagger_{k\sigma}\hat{a}_{k\sigma}$$
$$= \sum_{k\sigma}(\mathcal{H}_0)_k\,\hat{a}^\dagger_{k\sigma}\hat{a}_{k\sigma} \quad (11)$$

and, denoting $\hat{\rho}_q$ the Fourier component of the local density

$$\hat{A}_1(\boldsymbol{q}) = \sqrt{\frac{2\pi}{\Omega|\boldsymbol{q}|}}\frac{\hat{\rho}_q + \hat{\rho}_{-q}}{2} \quad \hat{A}_2(\boldsymbol{q}) = \sqrt{\frac{2\pi}{\Omega|\boldsymbol{q}|}}\frac{i\hat{\rho}_q - i\hat{\rho}_{-q}}{2}. \quad (12)$$

Operators (12) will be henceforth written as

$$\hat{A}_s(\boldsymbol{q}) = \sum_{kp\sigma}(\mathcal{A}_s(\boldsymbol{q}))_{kp}\,\hat{a}^\dagger_{k\sigma}\hat{a}_{p\sigma} \quad (13)$$

with

$$(\mathcal{A}_1(\boldsymbol{q}))_{kp} = \sqrt{\frac{2\pi}{\Omega|\boldsymbol{q}|}}\frac{\delta_{k,p+q} + \delta_{k,p-q}}{2},$$
$$(\mathcal{A}_2(\boldsymbol{q}))_{kp} = \sqrt{\frac{2\pi}{\Omega|\boldsymbol{q}|}}\frac{i\delta_{k,p+q} - i\delta_{k,p-q}}{2}. \quad (14)$$

Formulas (10)–(12) result from an exact calculation, immediately generalizable to all radial two-body interaction potentials, and to all spatial dimensionalities.

D. Numeric implementation

The observations outlined above give rise to a *polynomially complex* algorithm for numerically sampling (5), a pictorial representation of which is given in Fig. 1. Several Slater determinants $\{|\Psi_0^{(w)}\rangle\}_{w=1}^{N_w}$, called *walkers*, are initialized to the Hartree-Fock ground state, a filled Fermi sphere in the case of translationally invariant systems such as the 2D HEG, and given initial weights $\{\mathfrak{W}_0^{(w)}\}_{w=1}^{N_w}$ equal to 1.

Subsequently, each walker evolves under the action of operators (10) and its weight is updated through multiplication by (8). An estimate for the ground state of the system is provided by the following stochastic linear combination of Slater determinants:

$$|\Phi_0\rangle \simeq \frac{1}{\sum_{w=1}^{N_w}\mathfrak{W}_n^{(w)}}\sum_{w=1}^{N_w}\mathfrak{W}_n^{(w)}\frac{|\Psi_n^{(w)}\rangle}{\langle\Psi_T|\Psi_n^{(w)}\rangle}. \quad (15)$$
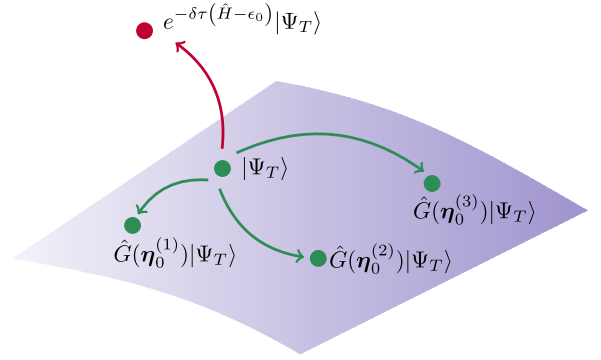

FIG. 1. Pictorial representation of the random walk in the manifold of N-particle Slater determinants $\mathfrak{D}(N)$ (lavender surface). The figure points out that the imaginary time propagator $e^{-\delta\tau(\hat{H}-\epsilon_0)}$ drives a Slater determinant $|\Psi_T\rangle$ away from $\mathfrak{D}(N)$, while the one-body propagators $\hat{G}(\boldsymbol{\eta})$ preserve $\mathfrak{D}(N)$. This permits us to retrieve the analytically intractable state $e^{-\delta\tau(\hat{H}-\epsilon_0)}|\Psi_T\rangle$ as a stochastic linear combination of Slater determinants $\hat{G}(\eta_0^{(w)})|\Psi_T\rangle$ according to (15).

Since numeric calculations can be carried out on finite-dimensional Hilbert spaces only, the numeric implementation of the phaseless AFQMC algorithm requires single-particle Hilbert space basis (2) of the system to be truncated, i.e., only the M lowest-energy plane-waves to be retained.

E. Dynamical correlation functions

The formalism outlined in Secs. II B and II D enables the calculation of ground state properties, and also of the ITCF,

$$F_{\hat{A},\hat{B}}(\tau) = \langle\Phi_0|\hat{A}e^{-\tau(\hat{H}-\epsilon_0)}\hat{B}|\Phi_0\rangle \quad (16)$$

of two one-body operators $\hat{A}, \hat{B}$. $F_{\hat{A},\hat{B}}(\tau)$ is related to the *dynamical* or *energy-resolved structure factor*

$$S_{\hat{A},\hat{B}}(\omega) = \int_{\mathbb{R}}dt\,\frac{e^{i\omega t}}{2\pi}\langle\Phi_0|\hat{A}(t)\hat{B}|\Phi_0\rangle \quad (17)$$

of $\hat{A}, \hat{B}$, a quantity appearing in linear response theory and providing precious information on the time-dependent response of the system to external fields. Dynamical structure factors and ITCFs are related to each other, as revealed by their Lehmann representation, by a Laplace transform.[8]

Within the AFQMC formalism, the issue of computing ITCFs is complicated by the circumstance that the one-body operators $\hat{A}, \hat{B}$ do not map Slater determinants onto Slater determinants, but on rather complicated states. Nevertheless, making use of the canonical anticommutation relations between fermionic creation and destruction operators, it is possible to show[19] that

$$e^{-\delta\tau(\hat{H}-\epsilon_0)}\hat{B} = \int dg(\boldsymbol{\eta})\,\hat{B}(\boldsymbol{\eta})\hat{G}(\boldsymbol{\eta}), \quad (18)$$

where $\hat{B}(\boldsymbol{\eta})$ is a suitable one-particle operator. In the case of the 2D HEG, it reads

$$\hat{B}(\boldsymbol{\eta}) = \sum_{kp\sigma}(\mathcal{B}(\boldsymbol{\eta}))_{kp}\,\hat{a}^\dagger_{k\sigma}\hat{a}_{p\sigma}, \quad (19)$$

where

$$\mathcal{B}(\boldsymbol{\eta}) = \mathcal{D}(\boldsymbol{\eta})\mathcal{B}\mathcal{D}(\boldsymbol{\eta})^{-1} \quad (20)$$

is defined through

$$(\mathcal{D}(\boldsymbol{\eta}))_{kp} = e^{-\frac{\delta\tau}{2}(\mathcal{H}_0)_k}\left(e^{-i\sqrt{\delta\tau}\sum_{qs}\eta_{qs}\mathcal{A}_s(q)}\right)_{kp} e^{-\frac{\delta\tau}{2}(\mathcal{H}_0)_p}. \quad (21)$$

By application of (18) and of the backpropagation technique,[19,32,33] it is possible to express the ITCF $F_{\hat{A},\hat{B}}(\tau)$ as mean value of a random variable over the random path followed by the walkers in the manifold of Slater determinants.

Further details of this calculation procedure are reported in Ref. 19. For the purpose of the present work, it is sufficient to recall that the phaseless AFQMC estimator of $F_{\hat{A},\hat{B}}(\tau)$ reads

$$
\begin{aligned}
F_{\hat{A},\hat{B}}(r\delta\tau) \simeq \frac{1}{\sum_{w=1}^{N_w}\mathfrak{W}_{m+n-r}^{(w)}} \\
\times \sum_{w=1}^{N_w}\sum_{ijkl}\mathcal{B}_{kl}\,\mathfrak{W}_{m+n}^{(w)}\frac{\langle\Psi_{BP,m}^{(w)}|\hat{A}\hat{a}_i^\dagger\hat{a}_j|\Psi_n^{(w)}\rangle}{\langle\Psi_{BP,m}^{(w)}|\Psi_n^{(w)}\rangle} \\
\times \mathcal{D}(\boldsymbol{\eta}_{n-1}^{(w)}-\boldsymbol{\xi}_{n-1}^{(w)},\dots,\boldsymbol{\eta}_{n-r}^{(w)}-\boldsymbol{\xi}_{n-r}^{(w)})_{ik} \\
\times \mathcal{D}^{-1}(\boldsymbol{\eta}_{n-1}^{(w)}-\boldsymbol{\xi}_{n-1}^{(w)},\dots,\boldsymbol{\eta}_{n-r}^{(w)}-\boldsymbol{\xi}_{n-r}^{(w)})_{lj}, \quad (22)
\end{aligned}
$$

where

$$|\Psi_{BP,m}^{(w)}\rangle = \hat{G}^\dagger(\boldsymbol{\eta}_n-\boldsymbol{\xi}_n)\dots\hat{G}^\dagger(\boldsymbol{\eta}_{n+m-1}-\boldsymbol{\xi}_{n+m-1})|\Psi_T\rangle \quad (23)$$

and

$$
\begin{aligned}
\mathcal{D}(\boldsymbol{\eta}_{n-1}^{(w)}-\boldsymbol{\xi}_{n-1}^{(w)},\dots,\boldsymbol{\eta}_{n-r}^{(w)}-\boldsymbol{\xi}_{n-r}^{(w)}) \\
= \mathcal{D}(\boldsymbol{\eta}_{n-1}^{(w)}-\boldsymbol{\xi}_{n-1}^{(w)})\dots\mathcal{D}(\boldsymbol{\eta}_{n-r}^{(w)}-\boldsymbol{\xi}_{n-r}^{(w)}). \quad (24)
\end{aligned}
$$

Estimator (22) is essentially a weighted average of suitably constructed matrix elements; each walker w constructs the matrix element and the weights $\mathfrak{W}_{m+n-r}^{(w)}$, $\mathfrak{W}_{m+n}^{(w)}$ involved in weighted average (22) from two Slater determinants $|\Psi_n^{(w)}\rangle$, $|\Psi_{BP,m}^{(w)}\rangle$ and two matrices $\mathcal{D}(\boldsymbol{\eta}_{n-1}^{(w)}-\boldsymbol{\xi}_{n-1}^{(w)},\dots,\boldsymbol{\eta}_{n-r}^{(w)}-\boldsymbol{\xi}_{n-r}^{(w)})$. These objects are functions of the auxiliary fields configurations $\boldsymbol{\eta}^{(w)}$ defining the random path followed by the walker in the manifold of Slater determinants, and their calculation is pictorially illustrated in Fig. 2.

In the present work, we consider the imaginary time density-density correlation function

$$F(\boldsymbol{q},\tau) = \frac{\langle\Phi_0|\hat{\rho}_{-\boldsymbol{q}}e^{-\tau(\hat{H}-\epsilon_0)}\hat{\rho}_{\boldsymbol{q}}|\Phi_0\rangle}{N} \quad (25)$$

which is the Laplace transform of the dynamical structure factor $S(\boldsymbol{q},\omega)$. This quantity is notoriously related to the differential cross section of electromagnetic radiation scattering and provides essential information for the quantitative description

of excitations of the HEG, collective charge density fluctuations, i.e., plasmons, end electron-hole excitations.[5,8]

For a finite system, $F(\boldsymbol{q},\tau)$ is a sum of exponentials with positive energies, corresponding to the excitations of the system.[5] To extract information about those excitation energies, it is, in general, necessary to compute $F(\boldsymbol{q},\tau)$ up to a sufficiently long imaginary time τ^*. To estimate the scaling of τ^* with r_s, we now make the assumption that $F(\boldsymbol{q},\tau)$ is a single exponential

$$F(\boldsymbol{q},\tau) \simeq S(\boldsymbol{q})\,e^{-\tau\omega(\boldsymbol{q})}, \quad (26)$$

with $\omega(\boldsymbol{q})$ equal to the plasmon dispersion relation that, for a 2D HEG,[5] in atomic units reads

$$\omega(\boldsymbol{q}) = \sqrt{2\pi n|\boldsymbol{q}|}. \quad (27)$$

Writing $n = \frac{N}{\Omega}$ and $\boldsymbol{q} = \frac{2\pi}{L}\boldsymbol{n}$, we find that $F(\boldsymbol{q},\tau)$ decays on a time scale τ^* proportional to $r_s^{3/2}$ and $N^{1/2}$. This qualitative estimate shows that the calculation of $F(\boldsymbol{q},\tau)$ becomes more and more demanding as r_s, N are increased. The assumption that $F(\boldsymbol{q},\tau)$ is equal to a single exponential is adequate only for small $|\boldsymbol{q}|$ and for a very large system. Otherwise, $F(\boldsymbol{q},\tau)$ is a sum of several exponentials. Some of those exponentials correspond to excitations in the particle-hole band and, for $|\boldsymbol{q}| \le 2k_F$, can have very low energy. Therefore, our estimate of τ^* is only a lower bound.

F. Numeric stabilization

In a previous work,[19] we have pointed out that estimator (22) is negatively conditioned by a form of numeric instability. The aim of the present section is to elucidate the origin of such phenomenon and to propose a method for stabilizing the calculation of ITCFs in AFQMC. AFQMC estimator (22) of the ITCF $F_{\hat{A},\hat{B}}(\tau)$ involves a weighted average, over the random paths followed by the N_w walkers employed in the simulation, of a quantity in which the matrix elements of $\mathcal{D}(\boldsymbol{\eta}_{n-1}^{(w)}-\boldsymbol{\xi}_{n-1}^{(w)},\dots,\boldsymbol{\eta}_{n-r}^{(w)}-\boldsymbol{\xi}_{n-r}^{(w)})$ and of its inverse appear. In the remainder of the present section, these matrices will be referred to as $\mathcal{D}$ and $\mathcal{D}^{-1}$ for brevity. The matrices $\mathcal{D}$ and $\mathcal{D}^{-1}$ need to be computed numerically, respectively, as product of r matrices and inverse of $\mathcal{D}$. It is well-known that the numerical computation of $\mathcal{D}$ and $\mathcal{D}^{-1}$ introduces rounding-off errors,[47] which accumulate as r increases with detrimental impact on the results of the computation.[16]

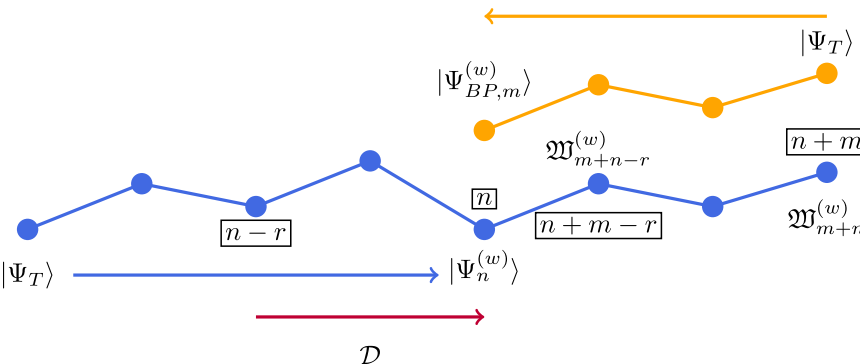Rounding-off errors are particularly severe when the ∞-norm condition number

FIG. 2. Pictorial representation of the phaseless AFQMC estimator for $F_{\hat{A},\hat{B}}(\tau)$, Equation (22); $F_{\hat{A},\hat{B}}(\tau)$ is computed at $\tau = r\,\delta\tau$ with $r = 2$, with $n = 5$ propagation steps and $m = 3$ backpropagation steps. The matrix $\mathcal{D}$ appearing in (24) is computed between the time steps $n - r$ and n (at which $|\Psi_n^{(w)}\rangle$ is computed); the determinant $|\Psi_{BP,m}^{(w)}\rangle$ is computed between the time steps n and $n + m$, and the weights $\mathfrak{W}_{m+n-r}^{(w)}$ and $\mathfrak{W}_{m+n}^{(w)}$ are computed at the time steps $m + n - r$ and $m + n$.

$$\kappa(\mathcal{D}) = \|\mathcal{D}\|_\infty \|\mathcal{D}^{-1}\|_\infty \qquad (28)$$

of the matrix $\mathcal{D}$, in which $\|A\|_\infty = \max_{ij} |A_{ij}|$ denotes the ∞-norm on the space of $M \times M$ complex-valued matrices, is large. For the systems under study, we observe a condition number roughly increasing as $\kappa(\mathcal{D}) \simeq C_1^r$ for some constant C_1. The rapid increase of $\kappa(\mathcal{D})$ indicates that the numeric matrix inversion $\mathcal{I}(\mathcal{D})$ used to estimate $\mathcal{D}^{-1}$ might be ill-conditioned, an intuition that can be confirmed by studying the figure of merit,

$$\|E\|_\infty = \|\mathbb{I} - \mathcal{D}\mathcal{I}(\mathcal{D})\|_\infty. \qquad (29)$$

For small r, $\frac{\|E\|_\infty}{M}$ is comparable with the machine precision $\epsilon = 10^{-16}$; it then increases as C_2^r for some constant C_2 and eventually saturates around 1. In Appendix B, a qualitative explanation of the power-law increase of $\frac{\|E\|_\infty}{M}$ is provided. The gradual corruption of data revealed by the increase of $\|E\|_\infty$ reflects, as illustrated in Fig. 3, on the quality of the AFQMC estimates of ITCFs, which combine the matrix elements of $\mathcal{D}$ and $\mathcal{I}(\mathcal{D})$ as prescribed by (22). We propose to mitigate the numeric instability of the ITCF estimator by performing a Tikhonov regularization[48] of the numeric inverse $\mathcal{I}(\mathcal{D})$. Practically, the SVD of $\mathcal{D}$ is computed,

$$\mathcal{D} = U \text{diag}(\sigma_1 \ldots \sigma_M) V^\dagger \qquad (30)$$

and $\mathcal{I}(\mathcal{D})$ is obtained as

$$\mathcal{I}(\mathcal{D}) = V \text{diag}(\tilde{\sigma}_1 \ldots \tilde{\sigma}_M) U^\dagger, \qquad (31)$$
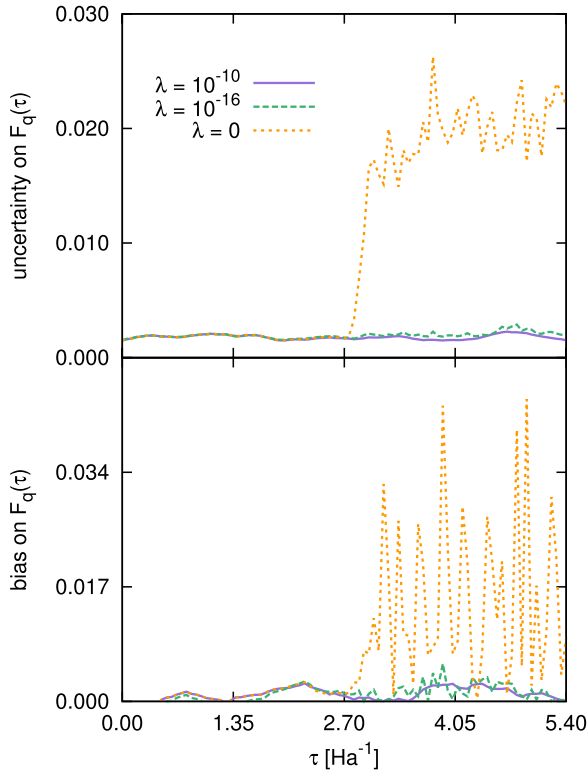

FIG. 3. Effect of Tikhonov regularization (31) on an ITCF relative to a system of $N = 2$ electrons with $M = 21$ basis set elements. Upper panel: statistical uncertainty affecting the AFQMC estimate of $F(q, \tau)$ with $\lambda = 10^{-10}$ (lavender solid lines), $\lambda = 10^{-16}$ (green dashed lines), and $\lambda = 0$ (orange dotted lines). Lower panel: bias affecting the AFQMC estimate of $F(q, \tau)$.

where $\tilde{\sigma}_i = \frac{\sigma_i}{\lambda^2 + \sigma_i^2}$ is defined by a regularization parameter λ. Large singular values $\sigma_i \gg \lambda$ are mapped to $\tilde{\sigma}_i \simeq \frac{1}{\sigma_i}$, while small singular values $\sigma_i \lesssim \lambda$ are kept below the threshold $\frac{1}{2\lambda}$. Particular care must be taken in choosing the regularization parameter λ, since for small λ the Tikhonov regularization is clearly ineffective, while for large λ it provokes a severe alteration in $\mathcal{I}(\mathcal{D})$. On the other hand, an intermediate value of λ prevents small errors in $\mathcal{D}$, associated to small singular values σ_i, to be dramatically amplified by the numeric inversion.

The effect of the Tikhonov regularization has been probed considering the model systems of 2 particles introduced in Ref. 19, for which exact numeric solution of the Hamiltonian eigenvalue problem is feasible, and thus the ITCFs are exactly known. In Fig. 3, we show the effect of Tikhonov regularization (31) on the ITCFs. The results show the existence of a broad interval of λ, comprising the machine precision $\epsilon = 10^{-16}$, for which the Tikhonov regularization mitigates the numeric instability affecting the AFQMC estimator of ITCFs without introducing any appreciable bias besides those coming from the real local energy and phaseless approximations. The figure displays, in the upper and lower panels, respectively, the statistical errors of the AFQMC estimations and the discrepancies with respect to the exact results for three different values of λ. It is evident that, as the imaginary time becomes large, the effect of the regularization is very important.

G. Computational cost

The AFQMC estimator of ITCFs should join numeric stability and low computational cost. The aim of the present section is to show that the computational cost of (22) is $O(M^3)$, M being the number of orbitals constituting the single-particle basis. The contribution F_w to (22) brought by a single walker of index w reads

$$F_w = \sum_{ijklrs} \mathcal{A}_{rs} \mathcal{B}_{kl} \langle \hat{a}_r^\dagger \hat{a}_s \hat{a}_i^\dagger \hat{a}_j \rangle_w \mathcal{D}_{ik} \mathcal{D}_{lj}^{-1}, \qquad (32)$$

where the abbreviation

$$\langle \cdot \rangle_w = \frac{\langle \Psi_{BP,m}^{(w)}| \cdot |\Psi_n^{(w)}\rangle}{\langle \Psi_{BP,m}^{(w)}|\Psi_n^{(w)}\rangle} \qquad (33)$$

has been inserted. The generalized Wick's theorem[19,49] implies that

$$\langle \hat{a}_r^\dagger \hat{a}_s \hat{a}_i^\dagger \hat{a}_j \rangle_w = \langle \hat{a}_r^\dagger \hat{a}_s \rangle_w \langle \hat{a}_i^\dagger \hat{a}_j \rangle_w + \langle \hat{a}_r^\dagger \hat{a}_j \rangle_w \langle \hat{a}_s \hat{a}_i^\dagger \rangle_w. \quad (34)$$

(34) is most conveniently expressed, introducing the definition $\mathcal{G}_{ij} = \langle \hat{a}_i^\dagger \hat{a}_j \rangle_w$ and recalling canonical anticommutation relations, as

$$\langle \hat{a}_r^\dagger \hat{a}_s \hat{a}_i^\dagger \hat{a}_j \rangle_w = \mathcal{G}_{rs}\mathcal{G}_{ij} + \mathcal{G}_{rj}(\delta_{is} - \mathcal{G}_{is}). \qquad (35)$$

Combining (32) and (35) yields

$$\begin{aligned} F_w = &\sum_{ijklrs} \mathcal{A}_{rs} \mathcal{B}_{kl} \mathcal{G}_{rs} \mathcal{G}_{ij} \mathcal{D}_{ik} \mathcal{D}_{lj}^{-1} \\ &+ \sum_{ijklr} \mathcal{A}_{ri} \mathcal{B}_{kl} \mathcal{G}_{rj} \mathcal{D}_{ik} \mathcal{D}_{lj}^{-1} \\ &- \sum_{ijklrs} \mathcal{A}_{rs} \mathcal{B}_{kl} \mathcal{G}_{rj} \mathcal{G}_{is} \mathcal{D}_{ik} \mathcal{D}_{lj}^{-1}. \end{aligned} \qquad (36)$$

Despite its cumbersome appearance, (36) can be efficiently evaluated computing the intermediate tensors $\mathcal{DB}$, $\mathcal{AG}^T$, and $\mathcal{D}^{-1}\mathcal{G}^T$ at the cost of $O(M^3)$ operations, and subsequently computing F_w as

$$
F_w = \left(\sum_r (\mathcal{AG}^T)_{rr} \right) \left(\sum_{il} (\mathcal{DB})_{il} (\mathcal{D}^{-1}\mathcal{G}^T)_{li} \right)
$$
$$
+ \sum_{ilr} (\mathcal{DB})_{il} (\mathcal{D}^{-1}\mathcal{G}^T)_{lr} \mathcal{A}_{ri}
$$
$$
- \sum_{ilr} (\mathcal{DB})_{il} (\mathcal{D}^{-1}\mathcal{G}^T)_{li} (\mathcal{AG}^T)_{ri} \qquad (37)
$$

at the cost of $O(M^3)$ more operations. The calculation of F_w further simplifies for operators $\hat{A}$ whose matrix elements read $\mathcal{A}_{ij} = \mathcal{A}_j \, \delta_{i,a(j)}$ for some function $a : \{1 \ldots M\} \to \{1 \ldots M\}$. The density fluctuation operator $\hat{\rho}_q = \sum_{k\sigma} \hat{a}^\dagger_{k+q\sigma} \hat{a}_{k\sigma}$ falls within such category.

The complexity $O(M^3)$ is the best allowed by the phaseless AFQMC methodology: in fact, the calculation of ITCFs requires at least $O(M^3)$ operations to accumulate the matrix $\mathcal{D}$, and the contractions in (36) do not compromise this favorable scaling with the number of single-particle orbitals.

III. RESULTS

The central results of this paper are (i) the practical verification of the possibility of accurately calculating *ab initio* ITCFs of medium-sized homogeneous electron gases and (ii) the understanding of the computational cost and limitations of the procedure. We have simulated paramagnetic systems of $N = 18, 26, 42$ electrons at $r_s = 0.1, 0.5, 1$; we show also results for $N = 18$ particles at $r_s = 2$. The complexity scales as M^3 (M being the number of basis sets elements), and the absolute statistical error of $F(\boldsymbol{q}, \tau)$ can be kept at the level 10^{-3}–2.5×10^{-3} with moderate computational resources even at values of $\tau \simeq 3/E_F$ for $r_s = 0.1, 0.5, 1$ and $\tau \simeq 2.5/E_F$ for $r_s = 2$, $E_F = 1/r_s^2$ being the Fermi energy.

The number N of electrons constituting the system is comparable to that used in the context of excited-states calculations through imaginary time correlation functions evaluated via configurational QMC methods reported in the literature.[24]

The imaginary time steps used in our calculations were $\delta\tau = 0.003, 0.004, 0.006, 0.008 \; E_{Ha}^{-1}$ at $r_s = 0.1, 0.5, 1, 2$, respectively. For each simulation, the number of plane-waves constituting the single-particle Hilbert space has been raised up to $M = 300$ according to the number of particles and to the strength of the interaction. For all calculations, it was verified that decreasing the time step and increasing the number of plane-waves had a negligible effect on the ground state energy per particle, which we illustrate in Table I, in comparison with RPA and configurational QMC. The configurational QMC evaluation of the ground state energy per particle has been performed using DMC, with a nodal structure encompassing backflow correlations optimized by means of the linear method.[39,40]

At $r_s = 0.1$, the three methods give compatible results. As r_s increases, AFQMC estimates are always closer to FN than RPA, lying between them. It is well-known that FN calcu-

TABLE I. RPA (column 3), AFQMC (column 4), and FN-DMC (column 5) estimates of the ground state energy for various systems (parameters are listed in columns 1-3); energies are measured in E_{Ha}. The RPA ground state energy is calculated on the Gaskell trial wavefunction.[50]

N	r_s	$\frac{\epsilon_0}{N}$ (RPA)	$\frac{\epsilon_0}{N}$ (AF)	$\frac{\epsilon_0}{N}$ (FN)
18	0.1	40.14	40.14(2)	40.13(1)
26	0.1	45.84	45.82(1)	45.81(1)
42	0.1	42.18	42.18(1)	42.17(1)
18	0.5	0.5065	0.5007(2)	0.5012(2)
26	0.5	0.7520	0.7360(2)	0.7326(8)
42	0.5	0.6031	0.6002(1)	0.5922(9)
18	1.0	−0.2489	−0.2562(1)	−0.2580(1)
26	1.0	−0.1847	−0.1921(1)	−0.1961(1)
42	1.0	−0.2215	−0.2283(1)	−0.2309(2)
18	2.0	−0.2661	−0.2695(1)	−0.2717(1)

lations with optimized nodal structures yield highly accurate estimates of the ground state energy, as confirmed by comparison with full configuration interaction QMC calculations:[53,54] this result, therefore, confirms the great accuracy of the phaseless approximation[55,56] in the sampling of the ground state wavefunction.

To obtain correct estimates of ITCFs, it is necessary to perform a sufficiently large number m of backpropagation steps. However, it is well-known[33] that raising m can result in an increase in variance, which severely limits the possibility of extracting physical information from the long imaginary-time tails of the ITCFs. We have used a number of backpropagation steps in the range $m = 200$–600. When $m = 600$ has proved insufficient, to avoid the increases in variance mentioned above, AFQMC estimates have been extrapolated to the $m \to \infty$ limit (data obtained by extrapolation will be henceforth marked with an asterisk).

A. Imaginary time correlation functions and excitation energies

For all the values of N and r_s, an AFQMC estimate of ITCF (25) is produced according to the procedure sketched in Section II E. The obtained $F(\boldsymbol{q}, \tau)$ is shown in the upper panel of Figs. 4–7. It is evident from the plots that the stabilization technique prevents an uncontrollable increase of the statistical error with imaginary time.

As it is well-known,[51] it is highly non-trivial to extract physical information from ITCFs. In the case of the HEG, the finite size of the systems under study induces to expect, for all the considered wave-vectors, contributions to $F(\boldsymbol{q}, \tau)$ coming from particle-hole excitations. The dynamical structure factor $S(\boldsymbol{q}, \omega)$, the inverse Laplace transform of $F(\boldsymbol{q}, \tau)$, is thus expected to display multiple peaks corresponding to the excitation energies. This picture is confirmed by RPA calculations for finite systems, reported in Appendix C.

The presence of multiple peaks complicates the task of performing the analytic continuation providing an estimate of $S(\boldsymbol{q}, \omega)$. Therefore, since the number of peaks grows rapidly with $|\boldsymbol{q}|$, we have limited our attention to the wave-vectors
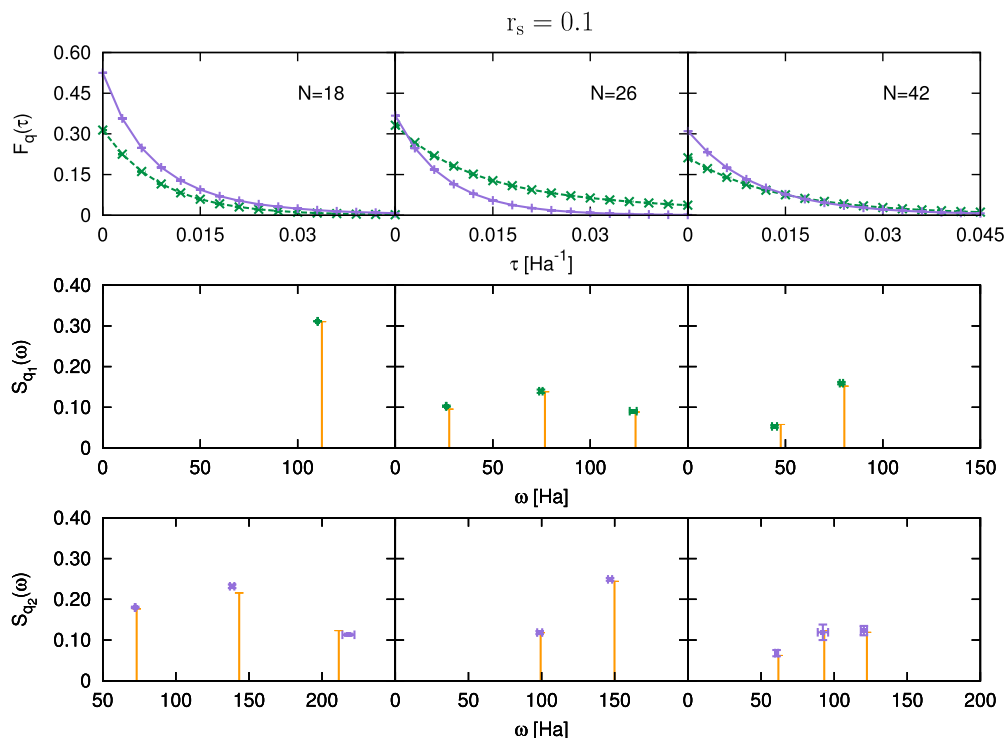
FIG. 4. Upper panel: imaginary time correlation functions of the density fluctuation operator $\hat{\rho}_q$ for paramagnetic systems of $N = 18, 26,$ and 42 particles (left to right) at $r_s = 0.1$, with transferred momenta q_1 (green dashed lines) and q_2 (lavender solid lines). When not visible, errors are smaller than the symbol size. Lines are only a guide for eyes. Central panel: dynamical structure factor for $N = 18, 26,$ and 42 particles (left to right) with transferred momentum q_1 (RPA: orange impulses, AFQMC: green symbols). Lower panel: dynamical structure factor for $N = 18, 26,$ and 42 particles (left to right) with transferred momentum q_2 (RPA: orange impulses, AFQMC: lavender symbols).
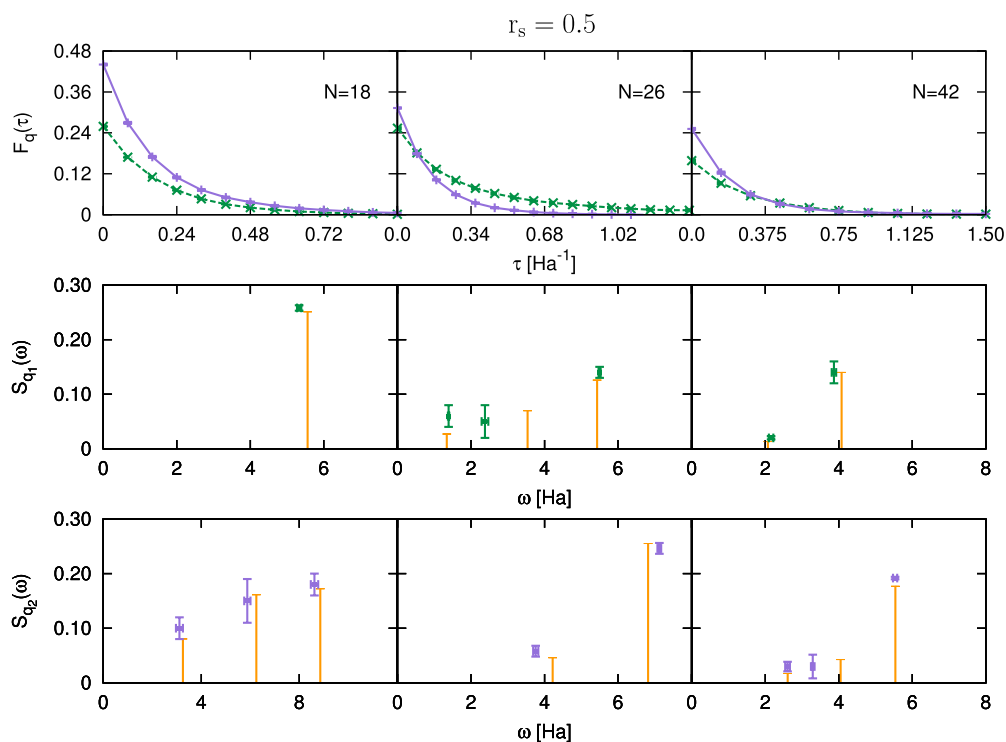

FIG. 5. Upper panel: imaginary time correlation functions of the density fluctuation operator $\hat{\rho}_q$ for paramagnetic systems of $N = 18, 26,$ and 42 particles (left to right) at $r_s = 0.5$, with transferred momenta q_1 (green dashed lines) and q_2 (lavender solid lines). When not visible, errors are smaller than the symbol size. Lines are only a guide for eyes. Central panel: dynamical structure factor for $N = 18, 26,$ and 42 particles (left to right) with transferred momentum q_1 (RPA: orange impulses, AFQMC: green symbols). Lower panel: dynamical structure factor for $N = 18, 26,$ and 42 particles (left to right) with transferred momentum q_2 (RPA: orange impulses, AFQMC: lavender symbols).
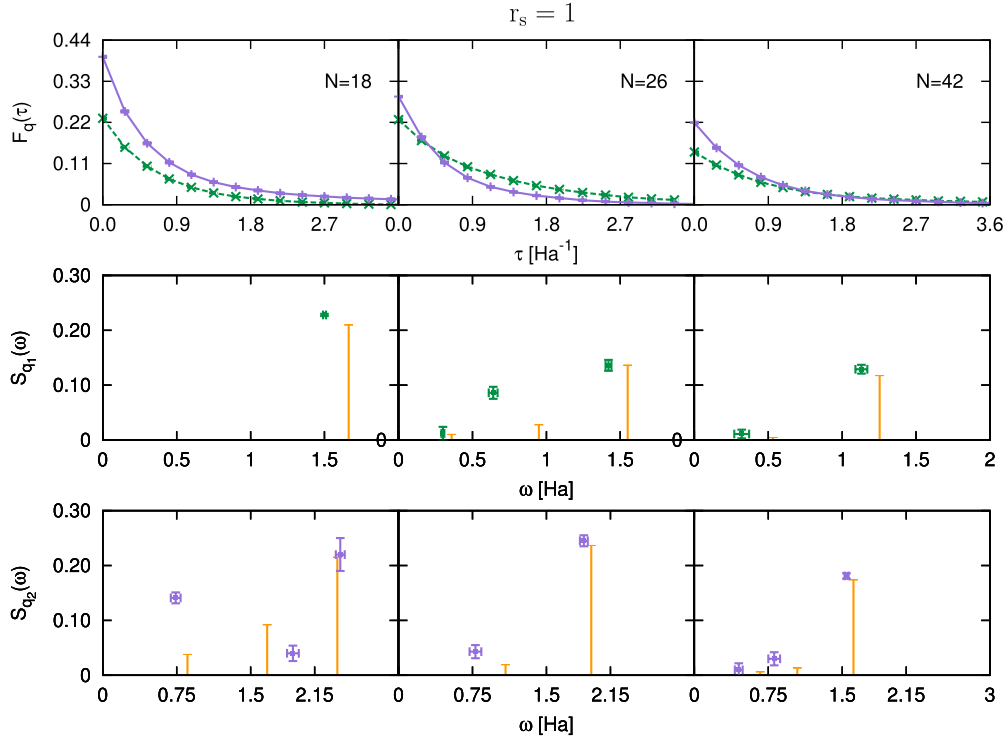
FIG. 6. Upper panel: imaginary time correlation functions of the density fluctuation operator $\hat{\rho}_q$ for paramagnetic systems of $N = 18, 26$, and 42 particles (left to right) at $r_s = 1$, with transferred momenta q_1 (green dashed lines) and q_2 (lavender solid lines). When not visible, errors are smaller than the symbol size. Lines are only a guide for eyes. Central panel: dynamical structure factor for $N = 18, 26$, and 42 particles (left to right) with transferred momentum q_1 (RPA: orange impulses, AFQMC: green symbols). Lower panel: dynamical structure factor for $N = 18, 26$, and 42 particles (left to right) with transferred momentum q_2 (RPA: orange impulses, AFQMC: lavender symbols).

$q_1 = (2\pi/L)(1, 0)$ and $q_2 = (2\pi/L)(1, 1)$. Notice that $|q_1|/k_F = 0.707, 0.5, 0.447$ and $|q_2|/k_F = 1, 0.707, 0.632$ for $N = 18, 26, 42$, respectively. Naturally, $k_F = \sqrt{2}/r_s$ is the Fermi wavevector. These low-momentum excitations are very interesting also from a physical point of view, in connection with the well-known collective plasmon excitation of the HEG.

For finite systems, the ITCF $F(q, \tau)$ is a sum of exponentials,

$$F(q, \tau) = \sum_{i=1}^{N_w} s_i e^{-\tau \omega_i} \qquad (38)$$

with positive frequencies ω_i and weights s_i. In particular, ω_i are the excitation frequencies of the system. Given our estimates of $F(q, \tau)$ we can only predict the $S(q, \omega)$ of the finite systems under study. For this reason, we do not attempt to predict the $S(q, \omega)$ in the thermodynamic limit, but limit ourselves to extract the excitations energies and weights by fitting the evaluated ITCF to a sum of exponentials with the well-established Levenberg-Marquardt curve-fitting method.[52] The number $N_w \le 3$ of frequencies and weights is that leading to the best fit.

In Figs. 4–7, we show results relative to the simulation of paramagnetic systems at $r_s = 0.1, 0.5, 1, 2$, respectively. Each figure contains data relative to the particle numbers $N = 18, 26, 42$ and wave-vectors q_1, q_2. In the upper panel, we show the estimated $F(q, \tau)$, while in the middle and lower panels we show, for q_1 and q_2, respectively, the obtained frequencies and weights, together with the RPA results. The AFQMC

estimations of the quantities s_i, ω_i are displayed as points with both horizontal and vertical statistical errors: the horizontal ones provide the uncertainties on the frequencies ω_i of the excitations, while the vertical ones give the error bars on the weights s_i. The coordinates of the points give, naturally, the mean frequencies and weights. The statistical uncertainties on the quantities s_i, ω_i are those yielded by the fit procedure. The frequencies predicted by the RPA are represented as impulses with height equal to the corresponding weights. Figs. 4–7 reveal that, for increasing r_s, $F(q, \tau)$ decays more and more slowly. In most cases, the dynamical structure factor exhibits a particle-hole excitation with energy roughly proportional to r_s^{-2}.

In order to extend this calculation to $r_s = 3$, we should compute $F(q, \tau)$ up to $\tau \simeq 25 E_{Ha}^{-1}$. Moreover, at $r_s = 2$, a calculation without numerical stabilization provides a reliable estimate of $F(q, \tau)$ for $\tau \le 5.5 E_{Ha}^{-1}$, and a stabilization with $\lambda = 10^{-16}$ brings this threshold to $\tau \le 10.0 E_{Ha}^{-1}$. On the basis of these observations, we expect that the calculation of $F(q, \tau)$ at $r_s > 3$ would be much more demanding and problematic, requiring a more aggressive stabilization. As a reference value, the calculations at $N = 18$ and $r_s = 1(2)$ required 6×10^3 (5×10^4) core hours on a Blue Gene/Q (Power BQC 1.6 GHz). The difference stems from the number of plane waves, of backpropagation steps and of imaginary time instants on which $F(q, \tau)$ has been computed. Based on these data, we expect that the calculation with $r_s = 3$ would require at least 2×10^5 core hours on the same facility.

We see that, at $r_s = 0.1$, there is a close agreement between AFQMC and RPA predictions of both frequencies and spectral
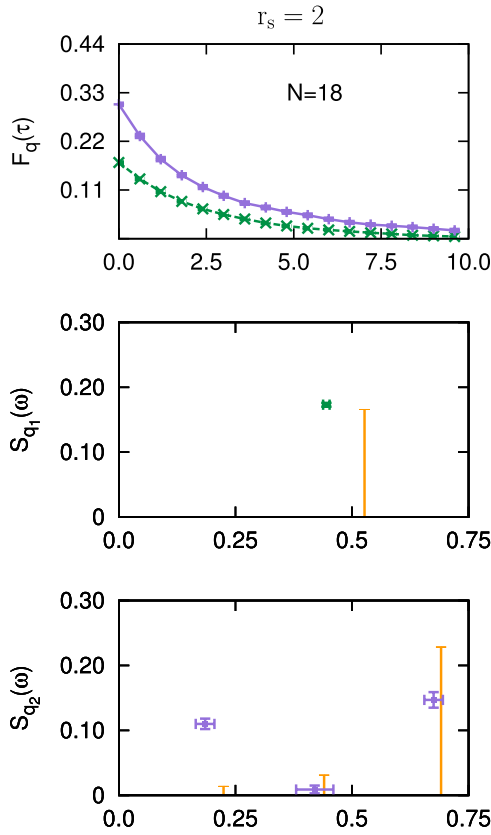
FIG. 7. Upper panel: imaginary time correlation functions of the density fluctuation operator $\hat{\rho}_q$ for paramagnetic systems of $N = 18, 26$, and 42 particles (left to right) at $r_s = 2$, with transferred momenta q_1 (green dashed lines) and q_2 (lavender solid lines). When not visible, errors are smaller than the symbol size. Lines are only a guide for eyes. Central panel: dynamical structure factor for $N = 18, 26$, and 42 particles (left to right) with transferred momentum q_1 (RPA: orange impulses, AFQMC: green symbols). Lower panel: dynamical structure factor for $N = 18, 26$, and 42 particles (left to right) with transferred momentum q_2 (RPA: orange impulses, AFQMC: lavender symbols).

weights. Since it is known that, for small r_s, RPA predictions are very accurate, such agreement provides a robust check for the reliability of AFQMC methodology in providing information about the manifold of excited states of the system. It is well known[19] that, in the same situation, calculations of $F(q, \tau)$ based on the fixed-node approximation would give inaccurate results even if the nodal structure of the ground state wavefunction is known with very high accuracy. As r_s increases, discrepancies appear between the two approaches. The presence of such discrepancies is naturally expected: none of the methodologies used in the present work is free from approximations. The approximations underlying RPA and AFQMC, in particular, are quite different in nature and are expected to agree only in the limit of high density (very low r_s).

In order to further assess the quality of our estimates of $F(q, \tau)$, we consider the momenta

$$\mathcal{M}_j = \int_0^\infty d\omega \, \omega^j \, S(q, \omega) \qquad j \in \mathbb{Z} \qquad (39)$$

of the dynamical structure factor. Indeed, several momenta $\mathcal{M}_j$ are fixed by sum rules[5] and can be compared with exact quantities or static properties. In particular,

$$\mathcal{M}_0 = S(q) \qquad (40)$$

TABLE II. Relative error (column 4) of first momentum (41), $\Delta\mathcal{M}_1 = |\mathcal{M}_1^{(AFQMC)} - \mathcal{M}_1| / \mathcal{M}_1$.

N	r_s	$|q|$	$\Delta\mathcal{M}_1$
18	0.1	8.355 427	0.015(9)
18	0.1	11.816 36	0.000(1)
26	0.1	6.952 136	0.001(1)
26	0.1	9.831 805	0.002(2)
42	0.1	5.469 911	0.003(4)
42	0.1	7.735 622	0.000(2)
18	0.5	1.671 085	0.015(21)
18	0.5	2.363 271	0.018(14)
26	0.5	1.390 427	0.006(6)
26	0.5	1.966 361	0.019(9)
42	0.5	1.093 982	0.023(38)
42	0.5	1.547 124	0.033(27)
18	1.0	0.835 543	0.020(11)
18	1.0	1.181 636	0.019(8)
26	1.0	0.695 214	0.036(16)
26	1.0	0.983 181	0.022(12)
42	1.0	0.546 991	0.002(10)
42	1.0	0.773 562	0.030(25)
18	2.0	0.417 771	0.078(21)
18	2.0	0.590 818	0.12(6)

while $\mathcal{M}_1$ obeys the continuity sum rule

$$\mathcal{M}_1 = \frac{|q|^2}{2} \qquad (41)$$

and $\mathcal{M}_{-1}$ obeys the compressibility sum rule

$$\mathcal{M}_{-1} = -\frac{\chi(q)}{2n}, \qquad (42)$$

where $\chi(q)$ denotes the static density response function.

In Table II, we compute momentum (41) using the dynamical structure factors in Figs. 4–7 and we compare it with the exact value $|q|^2/2$. In most cases, the AFQMC estimate of (41) is less than 2 standard deviations away from the exact result. We remark that, unlike in the case of RPA, there is no *a priori* motivation for expecting that AFQMC estimators of density-density ITCFs provide accurate estimates of the first momentum.

In order to further assess the quality of our results, in Tables III and IV, we detail the comparison with the RPA and configurational QMC results for the static structure factor $S(q) = F(q, 0)$ and the static density response function

$$\tilde{\chi}(q) = -\frac{\chi(q)}{2n} = \int_0^{+\infty} d\tau \, F(q, \tau) = \mathcal{M}_{-1}. \qquad (43)$$

In the AFQMC calculations, $\tilde{\chi}(q)$ is obtained using the dynamical structure factors in Figs. 4–7. In absence of exact results for ITCFs, the comparison between QMC estimates of static properties related to the momenta of $S(q, \omega)$ is a practical way of assessing the quality of ITCFs from AFQMC calculations.

The configurational QMC evaluation of the static structure factor $S(q)$ has been obtained via FN DMC calculations with the nodal structure described above. The DMC estimates are calculated using the extrapolated estimator.[42] We observe that, increasing r_s above 0.1, the AFQMC predictions remain, in

TABLE III. RPA (column 4), AFQMC (column 5), and FN-DMC (column 6) estimates of the static structure factor $S(q)$ for various systems and wave-vectors (parameters are listed in columns 1-3); wave-vectors are measured in a_B^{-1}.

N	r_s	$|q|$	$S(q)$ (RPA)	$S(q)$ (AF)	$S(q)$ (FN)
18	0.1	8.355 427	0.3105	0.314(2)	0.319(4)
18	0.1	11.816 36	0.5150	0.525(4)	0.521(4)
26	0.1	6.952 136	0.3326	0.342(2)	0.343(4)
26	0.1	9.831 805	0.3623	0.367(6)	0.370(5)
42	0.1	5.469 911	0.2101	0.212(7)	0.217(4)
42	0.1	7.735 622	0.3045	0.310(6)	0.306(5)
18	0.5	1.671 085	0.2511	0.258(1)	0.266(4)
18	0.5	2.363 271	0.4137	0.440(3)	0.448(5)
26	0.5	1.390 427	0.2225	0.254(3)[a]	0.238(4)
26	0.5	1.966 361	0.3009	0.313(2)	0.322(4)
42	0.5	1.093 982	0.1533	0.161(2)	0.146(5)
42	0.5	1.547 124	0.2366	0.247(2)	0.264(4)
18	1.0	0.835 543	0.2098	0.231(2)	0.218(5)
18	1.0	1.181 636	0.3451	0.395(3)	0.386(4)
26	1.0	0.695 214	0.1746	0.227(2)[a]	0.192(5)
26	1.0	0.983 181	0.2558	0.289(2)	0.281(4)
42	1.0	0.546 991	0.1219	0.141(1)	0.126(5)
42	1.0	0.773 562	0.1938	0.219(2)	0.208(5)
18	2.0	0.417 771	0.1657	0.172(2)[a]	0.176(4)
18	2.0	0.590 818	0.2732	0.304(3)[a]	0.305(4)

[a]AFQMC estimates are extrapolated.

TABLE IV. RPA (column 4), AFQMC (column 5), and FN-DMC (column 6) estimates of the compressibility $\tilde{\chi}(q)$ for various systems and wave-vectors (parameters are listed in columns 1-3; and $\tilde{\chi}(q)$ in E_{Ha}^{-1}.

N	r_s	$|q|$	$\tilde{\chi}(q)$ (RPA)	$\tilde{\chi}(q)$ (AF)	$\tilde{\chi}(q)$ (FN)
18	0.1	8.355 427	0.002 76	0.0028(4)	0.002 87(1)
18	0.1	11.816 36	0.004 49	0.0046(1)	0.004 69(1)
26	0.1	6.952 136	0.005 98	0.0065(2)	0.006 53(4)
26	0.1	9.831 805	0.002 82	0.0028(1)	0.002 87(4)
42	0.1	5.469 911	0.003 11	0.0032(4)	0.003 25(4)
42	0.1	7.735 622	0.003 30	0.0034(2)	0.003 35(2)
18	0.5	1.671 085	0.045 16	0.048(1)	0.048 4(4)
18	0.5	2.363 271	0.069 92	0.081(2)	0.078 8(4)
26	0.5	1.390 427	0.062 98	0.085(6)[a]	0.069(2)
26	0.5	1.966 361	0.048 27	0.051(1)	0.050 4(4)
42	0.5	1.093 982	0.040 74	0.043(5)	0.042(2)
42	0.5	1.547 124	0.049 03	0.051(3)	0.049(2)
18	1.0	0.835 543	0.126 12	0.152(3)	0.143(2)
18	1.0	1.181 636	0.189 79	0.301(6)	0.226(1)
26	1.0	0.695 214	0.146 01	0.22(2)[a]	0.162(2)
26	1.0	0.983 181	0.138 72	0.188(6)	0.161(2)
42	1.0	0.546 991	0.102 12	0.158(7)	0.14(1)
42	1.0	0.773 562	0.130 14	0.176(9)	0.16(1)
18	2.0	0.417 771	0.314 51	0.34(1)[a]	0.374(4)
18	2.0	0.590 818	0.462 38	0.89(1)[a]	0.590(2)

[a]AFQMC estimates are extrapolated.

general, closer to the configurational QMC ones than to the RPA ones: this is a further verification about the quality of the phaseless AFQMC and of the backpropagation technique.

Even more significant is the comparison between AFQMC estimates of the static density response function $\tilde{\chi}(q)$, which we obtain from momentum (42) of the dynamical structure factor, with RPA and fixed-node estimations. In principle, the fixed-node evaluation of the static density response function $\tilde{\chi}(q)$ is highly non-trivial, involving the manifold of excited states. However, it is well-known that this difficulty can be circumvented[11] extracting $\tilde{\chi}(q)$ from the ground state energy $E(v_q)$ of a system subject to an external periodic potential of amplitude v_q in the $v_q \to 0$ limit. Again, increasing r_s above 0.1, the AFQMC predictions remain, in general, closer to the configurational Monte Carlo ones than to the RPA ones: this is a strong indication about the quality of AFQMC results, since the FN QMC calculations include correlations beyond the RPA level.

This result is remarkable, since the AFQMC evaluation of $\tilde{\chi}(q)$ is considerably influenced by the low-energy excitations which, if predicted inaccurately, can significantly bias the result. We notice that knowledge of momenta (40)–(42) was not enforced in the fitting procedure that led us to the dynamical structure factor: instead, those quantities have been computed from the dynamical structure factor and found in satisfactory agreement, at least for $r_s \leq 1$, with independently derived quantities.

The study of momenta (40) and (42) leads to argue that the deviations from the RPA observed at $r_s \leq 1$ indicate the better accuracy of the AFQMC dynamical structure factor. Indeed, the configurational QMC includes correlations beyond the RPA level, and thus its estimate of momenta (40) and (42) should be considered more accurate than RPA estimates. Since the AFQMC dynamical structure factor leads to estimates of (40) and (42) which are in better agreement with FN QMC, at least for $r_s \leq 1$, we argue that AFQMC provides more accurate estimates of $F(q, \tau)$ and thus $S(q, \omega)$ than RPA. This result shows that, remarkably, in the high-density regime the accuracy of AFQMC for the imaginary time dynamics is comparable to that of the ground state energy.

As r_s further increases, however, the agreement decreases. We have verified that the number of plane-waves and the number of backpropagation steps are sufficiently large to extrapolate the results and to filter the excited states contributions from the trial wavefunction. Hence, the origin of the discrepancies between the estimations yield by the three methodologies used in the present work has to be sought in the approximation schemes underlying them.

IV. CONCLUSIONS

We have shown the possibility to provide accurate first principles calculations of imaginary time correlations for medium-sized fermionic systems in the continuum, using the phaseless auxiliary field quantum Monte Carlo method.

We have simulated a $2D$ homogeneous electron gas of up to $N = 42$ electrons using a plane-waves basis set of up to $M = 300$ elements. We have shown that the density-density correlation function in imaginary time can be calculated via

a polynomially complex algorithm with the favorable scaling $O(M^3)$. In order to achieve a good accuracy level in the calculations, we propose stabilization procedures to deal with matrix inversion, which can be used in combination with well-established stabilization procedures for matrix exponentiation and multiplication:[57,58] in particular, we suggest a Tikhonov regularization that allows to maintain a good accuracy level even for imaginary time values of the order of $3/E_F$. We have yielded also comparisons with predictions of the static structure factor and the static density response obtained via the RPA approximation and via fixed-node quantum Monte Carlo calculations.

At small r_s, the AFQMC correctly reproduces the RPA results. At larger r_s on the other hand, it provides quantitative estimates of the deviations from the RPA, as the comparison with FN calculations reveals. We believe this is a relevant result for QMC simulations: it is known, in fact, that the widely employed fixed-node approximation fails to properly sample the imaginary-time propagator, due to the imposition of the ground-state nodal structure to excited states.[19] AFQMC, on the other hand, appears to provide a useful tool to explore, from first principles, the manifold of the excited states of a fermionic system. In particular, our calculations qualify the phaseless AFQMC as a practical and useful methodology for the accurate evaluation of $F(q, \tau)$, for homogeneous systems of $N = O(10^2)$ correlated fermions in the continuum. Calculations are lighter and more accurate when ITCFs decay rapidly, as in the case of 2D HEGs in the high-density regime. To further assess the performance of the methodology, it would be relevant to compute other ITCFs for both homogeneous and non-homogeneous systems, such as chemical systems.

ACKNOWLEDGMENTS

APPENDIX A: HUBBARD-STRATONOVICH TRANSFORMATION FOR THE 2D HEG

By a straightforward application of the canonical anticommutation relations, Hamiltonian (1) can be exactly rewritten as

$$\hat{H} = \sum_{k\sigma} \left(\frac{|k|^2}{2} - \mu(k) \right) \hat{a}_{k\sigma}^\dagger \hat{a}_{k\sigma} + \frac{1}{2\Omega} \sum_q \frac{2\pi}{|q|} \hat{\rho}_q \hat{\rho}_{-q}, \quad (A1)$$

where

$$\mu(k) = \frac{1}{2\Omega} \sum_{p \neq k} \frac{2\pi}{|p - k|} \quad (A2)$$

and $\hat{\rho}_q = \sum_{k\sigma} \hat{a}_{k-q\sigma}^\dagger \hat{a}_{k\sigma}$ is the density fluctuation operator. Recalling the parity of $\frac{2\pi}{|q|}$ and the anticommutation relation

$$[\hat{\rho}_q, \hat{\rho}_{-q}]_+ = \frac{(\hat{\rho}_q + \hat{\rho}_{-q})^2}{2} + \frac{(i\hat{\rho}_q - i\hat{\rho}_{-q})^2}{2}, \quad (A3)$$

one eventually finds

$$\hat{H} = \hat{H}_0 + \frac{1}{2} \sum_q \left(\hat{A}_1(q)^2 + \hat{A}_2(q)^2 \right) \quad (A4)$$

with

$$\hat{H}_0 = \sum_{k\sigma} \left(\frac{|k|^2}{2} - \mu(k) \right) \hat{a}_{k\sigma}^\dagger \hat{a}_{k\sigma} \quad (A5)$$

and

$$\hat{A}_1(q) = \sqrt{\frac{2\pi}{\Omega|q|}} \frac{\hat{\rho}_q + \hat{\rho}_{-q}}{2} \quad \hat{A}_2(q) = \sqrt{\frac{2\pi}{\Omega|q|}} \frac{i\hat{\rho}_q - i\hat{\rho}_{-q}}{2} \quad (A6)$$

which, since $\hat{\rho}_{-q} = \hat{\rho}_q^\dagger$, are hermitian operators. Applying the Hubbard-Stratonovich transformation to the propagator of Hamiltonian (11) yields

$$\hat{G}(\eta) = e^{-\frac{\delta\tau}{2}\hat{H}_0} e^{-i\sqrt{\delta\tau}\sum_q \eta_{1q}\hat{A}_1(q) + \eta_{2q}\hat{A}_2(q)} e^{-\frac{\delta\tau}{2}\hat{H}_0}. \quad (A7)$$

APPENDIX B: NUMERIC STABILITY OF MATRIX INVERSION

The distance

$$\|\mathcal{I}(\mathcal{D}_r) - \mathcal{D}_r^{-1}\|_\infty \quad (B1)$$

between the actual inverse $\mathcal{D}_r^{-1}$ of $\mathcal{D}_r$ and its numeric estimate $\mathcal{I}(\mathcal{D}_r)$ (B1) is bounded[47] by

$$\|\mathcal{I}(\mathcal{D}_r) - \mathcal{D}_r^{-1}\|_\infty \leq M\|\mathcal{I}(\mathcal{D}_r)\|_\infty \frac{\|E_r\|_\infty}{1 - M\|E_r\|_\infty} \quad (B2)$$

with

$$\|E_r\|_\infty = \|\mathbb{I} - \mathcal{D}_r \mathcal{I}(\mathcal{D}_r)\|_\infty. \quad (B3)$$

Equation (B2) holds for $\|E_r\|_\infty < \frac{1}{M}$ and is therefore adequate to the description of $\|E_r\|_\infty$ for small r. It can be combined with the following estimate:[59]

$$\|\mathcal{I}(\mathcal{D}_r) - \mathcal{D}_r^{-1}\|_\infty \simeq \epsilon\|\mathcal{D}_r^{-1}\|_\infty^2 \frac{M^3}{3} \quad (B4)$$

to yield

$$M\|E_r\|_\infty \simeq \frac{\epsilon \frac{M^3}{3} \|\mathcal{D}_r^{-1}\|_\infty^2}{\|\mathcal{I}(\mathcal{D}_r)\|_\infty + \epsilon \frac{M^3}{3} \|\mathcal{D}_r^{-1}\|_\infty^2}. \quad (B5)$$

In the case of AFQMC calculations, where $\mathcal{D}_r$ and $\mathcal{D}_r^{-1}$ come from the product of r matrices,

$$\|\mathcal{D}_r^{-1}\|_\infty = C_3^r \quad \|\mathcal{I}(\mathcal{D}_r)\|_\infty = C_4^r, \quad (B6)$$

where C_3 and C_4 are suitable constants, close to each other. Merging (B4) and (B6) leads to

$$\|E_r\|_\infty \simeq \frac{\epsilon \frac{M^2}{3}}{\left(\frac{C_4}{C_3^2}\right)^r + \epsilon \frac{M^3}{3}} \quad (B7)$$

which reduces to

$$\|E_r\|_\infty \simeq \epsilon \frac{M^2}{3} \left(\frac{C_3^2}{C_4} \right)^r \quad (B8)$$

in the limit of small r. Since $C_4 < C_3^2$, C_3 and C_4 being close to each other, estimate (B8) leads to a power-law increase of $\|E_r\|_\infty$.

APPENDIX C: RPA FOR FINITE HOMOGENEOUS SYSTEMS

The aim of this appendix is to provide a brief description of the RPA[5,8,37] for finite interacting systems and of the procedure leading to the excitation energies and weights, with which AFQMC results have been compared.

The RPA can be regarded to Ref. 8 as a refinement of the well-known Tamm-Dancoff approximation[8,60,61] (TDA), which has long been supporting the study of excitations in nuclear systems. The TDA relies on the assumptions that the ground state of the system is the Hartree-Fock determinant, and that excited states can be represented as superpositions of determinants obtained promoting a single particle above the Fermi surface. Within RPA, on the other hand, a better approximation $|\Phi_0\rangle$ for the actual ground state of the interacting system is employed to build up an Ansatz for plasmonic wavefunctions. To this purpose, the distinction between spin-orbitals below and above the Fermi level is made explicit by writing

$$\hat{a}_{k\sigma}^\dagger = \begin{cases} \hat{c}_{k\sigma}^\dagger & \text{if } |k| > k_F \\ \hat{b}_{k\sigma} & \text{if } |k| \le k_F \end{cases} \tag{C1}$$

and Hamiltonian (1) is consequently expressed as

$$\begin{aligned} \hat{H} &= \hat{T} + \hat{V} \\ &= \sum_{k\sigma} t_k \, \hat{c}_{k\sigma}^\dagger \hat{c}_{k\sigma} + \sum_{k\sigma} t_k \left(1 - \hat{b}_{k\sigma}^\dagger \hat{b}_{k\sigma} \right) \\ &\quad + \frac{1}{2\Omega} \sum_{q \ne 0} \phi_q \hat{\rho}_q \hat{\rho}_{-q}, \end{aligned} \tag{C2}$$

where $t_k = \frac{|k|^2}{2}$, $\phi_q = \frac{2\pi}{|q|}$, the first sum goes over all wave-vectors k such that $|k| > k_F$, the second sum goes over all wave-vectors k such that $|k| \le k_F$, and the density fluctuation

operator $\hat{\rho}_q$ is approximated[37] by

$$\hat{\rho}_q \simeq \sum_{k\sigma} \hat{c}_{k+q\sigma}^\dagger \hat{b}_{k\sigma}^\dagger + \hat{b}_{k+q\sigma}^\dagger \hat{c}_{k\sigma}, \tag{C3}$$

where the first sum, describing forward scattering processes in which a particle is promoted above the Fermi level, goes over all wave-vectors k such that $|k| > k_F$ and $|k + q| \le k_F$, and the second sum, describing backward scattering processes in which a particle is brought back below the Fermi level, goes over all wave-vectors k such that $|k| \le k_F$ and $|k + q| > k_F$. The RPA Ansatz for plasmonic wavefunctions is

$$|\Phi_q\rangle = \sum_{k\sigma} X_k \hat{c}_{k+q\sigma}^\dagger \hat{b}_{k\sigma}^\dagger |\Phi_0\rangle + \sum_{k\sigma} Y_k \hat{b}_{k+q\sigma}^\dagger \hat{c}_{k\sigma} |\Phi_0\rangle. \tag{C4}$$

(C4) is justified by the observation that the pair destruction operator $\hat{b}_{k+q\sigma}\hat{c}_{k\sigma}$ annihilates the Hartree-Fock determinant but not the actual ground state of the interacting system. The eigenvalues ϵ such that $\hat{H}|\Phi_q\rangle = \epsilon|\Phi_q\rangle$ are obtained recalling that the commutators between the Coulomb interaction and the pair creation and destruction operators can be approximated[37] as

$$[\hat{c}_{k+q\sigma}^\dagger \hat{b}_{k\sigma}^\dagger, \hat{V}] \simeq -\frac{\phi_q}{\Omega} \hat{\rho}_q \tag{C5}$$

and

$$[\hat{b}_{k+q\sigma}\hat{c}_{k\sigma}, \hat{V}] \simeq \frac{\phi_q}{\Omega} \hat{\rho}_q, \tag{C6}$$

respectively. Now, since $|\Phi_0\rangle$ and $|\Phi_q\rangle$ and eigenstates of $\hat{H}$ with eigenvalues ϵ_0 and $\epsilon = \epsilon_0 + \Delta\epsilon$, respectively, the following identity holds

$$\begin{aligned} 0 &= \langle\Phi_q|(\epsilon - \hat{H})\,\hat{c}_{k+q\sigma}^\dagger \hat{b}_{k\sigma}^\dagger|\Phi_0\rangle \\ &= \Delta\epsilon \, \langle\Phi_q|\hat{c}_{k+q\sigma}^\dagger \hat{b}_{k\sigma}^\dagger|\Phi_0\rangle - \langle\Phi_q|[\hat{H}, \hat{c}_{k+q\sigma}^\dagger \hat{b}_{k\sigma}^\dagger]|\Phi_0\rangle \end{aligned} \tag{C7}$$

from which

$$\langle\Phi_q|\hat{c}_{k+q\sigma}^\dagger \hat{b}_{k\sigma}^\dagger|\Phi_0\rangle = \frac{\frac{\phi_q}{\Omega}\langle\Phi_q|\hat{\rho}_q|\Phi_0\rangle}{\Delta\epsilon + t_k - t_{k+q}} \tag{C8}$$

follows. Similarly,

$$\langle\Phi_q|\hat{b}_{k+q\sigma}\hat{c}_{k\sigma}|\Phi_0\rangle = -\frac{\frac{\phi_q}{\Omega}\langle\Phi_q|\hat{\rho}_q|\Phi_0\rangle}{\Delta\epsilon + t_k - t_{k+q}}. \tag{C9}$$

Equations (C8) and (C9) can be summed over k, σ to yield the secular equation

$$\langle\Phi_q|\hat{\rho}_q|\Phi_0\rangle = \frac{2\phi_q}{\Omega}\langle\Phi_q|\hat{\rho}_q|\Phi_0\rangle \left(\sum_{\substack{|k| \le k_F \\ |k+q| > k_F}} \frac{1}{\Delta\epsilon + t_k - t_{k+q}} - \sum_{\substack{|k| > k_F \\ |k+q| \le k_F}} \frac{1}{\Delta\epsilon + t_k - t_{k+q}} \right) \tag{C10}$$

which, simplifying the matrix element $\langle\Phi_q|\hat{\rho}_q|\Phi_0\rangle$ in both members, and applying the change of variables $r = -k - q$ in the second sum, takes the form

$$1 = \frac{\phi_q}{\Omega}\left[2 \sum_{\substack{|k| \le k_F \\ |k+q| > k_F}} \frac{1}{t_k - t_{k+q} + \Delta\epsilon} + \frac{1}{t_k - t_{k+q} - \Delta\epsilon} \right], \tag{C11}$$
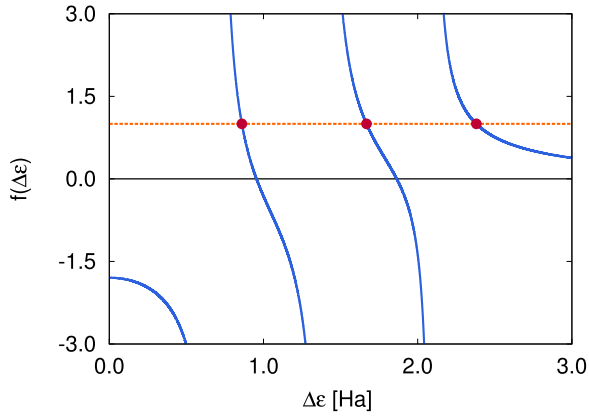
FIG. 8. RPA secular equation for a paramagnetic system of $N = 18$ particles at $r_s = 1$, and $\boldsymbol{q}_2$. The blue solid line is the right member $f(\Delta\epsilon)$ of (C11), and the orange dashed line is the constant function $g(\Delta\epsilon) = 1$; intersections between the two graphs are marked with red dots. The RPA eigenvalues are the abscissas of such intersections.

where the term between square brackets is immediately identified with the real part of the $2D$ Lindhard function $\chi_0(\boldsymbol{q}, \Delta\epsilon)$.[5] The coefficients X_k, Y_k are determined substituting (C4) in (C8) and (C9), and read

$$X_k = \frac{\mathcal{N}}{t_k - t_{k+q} + \Delta\epsilon},$$
$$Y_k = -\frac{\mathcal{N}}{t_k - t_{k+q} + \Delta\epsilon}, \qquad \text{(C12)}$$

where $\mathcal{N}$ is a normalization constant. Notice that X_k is defined for $|\boldsymbol{k}| \leq k_F$, $|\boldsymbol{k} + \boldsymbol{q}| > k_F$ while Y_k for $|\boldsymbol{k}| > k_F$ and $|\boldsymbol{k} + \boldsymbol{q}| \leq k_F$. The right-hand side of (C11) is a function $f(\Delta\epsilon) = \frac{\phi_q}{\Omega} \chi_0(\boldsymbol{q}, \Delta\epsilon)$, illustrated in Fig. 8, with the following properties:

$$\lim_{\Delta\epsilon \to 0} f(\Delta\epsilon) < 0,$$
$$\lim_{\Delta\epsilon \to +\infty} f(\Delta\epsilon) = 0^+ \qquad \text{(C13)}$$

and diverging in correspondence to the particle-hole energies $t_{k+q} - t_k$. As a consequence, there exists a root of secular equation (C11) between all the poles of $f(\Delta\epsilon)$ and another root above them. The excited state corresponding to this root has coefficients X_k, Y_k sharing the same sign and is therefore a coherent superposition of particle-hole excitations describing a collective high-energy oscillation being precursive of the plasmon. The excited states corresponding to other roots of (C11) have coefficients X_k, Y_k with non-constant sign, and therefore take into account the persistence of non-interacting properties in the spectrum of the electron gas, even in presence of Coulomb interaction.

We have seen that the RPA approximation yields an Ansatz for the energies $\epsilon_{q,n}$ and wavefunctions $|\Phi_{q,n}\rangle$ of excited states with definite momentum $\boldsymbol{q}$, which results in the following approximation for the image of the RPA ground state through the density fluctuation operator $\hat{\rho}_q$:

$$\hat{\rho}_q |\Phi_0\rangle = \sum_n |\Phi_{q,n}\rangle\langle\Phi_{q,n}|\hat{\rho}_q|\Phi_0\rangle \qquad \text{(C14)}$$

with

$$\langle\Phi_{q,n}|\hat{\rho}_q|\Phi_0\rangle = \sum_{\substack{|\boldsymbol{k}| \leq k_F \\ |\boldsymbol{k}+\boldsymbol{q}| > k_F}} X_{k,n} + \sum_{\substack{|\boldsymbol{k}| > k_F \\ |\boldsymbol{k}+\boldsymbol{q}| \leq k_F}} Y_{k,n} \qquad \text{(C15)}$$

and for the dynamical structure factor,

$$S(\boldsymbol{q}, \omega) = \frac{1}{N} \sum_n \delta(\omega - \epsilon_{q,n})|\langle\Phi_{q,n}|\hat{\rho}_q|\Phi_0\rangle|^2. \qquad \text{(C16)}$$

[1] E. P. Wigner, Phys. Rev. **46**, 1002 (1934).
[2] F. Bloch, Z. Phys. **57**, 549 (1929).
[3] A. W. Overhauser, Phys. Rev. Lett. **3**, 414 (1959).
[4] D. Ceperley, Phys. Rev. B **18**, 3126 (1978); D. M. Ceperley and B. J. Alder, Phys. Rev. Lett. **45**, 566 (1980).
[5] G. F. Giuliani and G. Vignale, *Quantum Theory of the Electron Liquid* (Cambridge University Press, 2005).
[6] S. Zhang and D. Ceperley, Phys. Rev. Lett. **100**, 236404 (2008).
[7] For a comprehensive review of the existing quantum chemistry methodologies see for example the book, A. Szabo and N. S. Ostlund, *Modern Quantum Chemistry: Introduction to Advanced Electronic Structure Theory* (Dover Publications, 1996).
[8] A. L. Fetter and J. D. Walecka, *Quantum Theory of Many-Particle Systems* (Dover, 2003).
[9] B. Tanatar and D. M. Ceperley, Phys. Rev. B **39**, 5005 (1989).
[10] Y. Kwon, D. M. Ceperley, and R. M. Martin, Phys. Rev. B **48**, 12037 (1993).
[11] S. Moroni, D. M. Ceperley, and G. Senatore, Phys. Rev. Lett. **75**, 689 (1995).
[12] M. Padmanabhan, T. Gokmen, N. C. Bishop, and M. Shayegan, Phys. Rev. Lett. **101**, 026402 (2008).
[13] T. Gokmen, M. Padmanabhan, K. Vakili, E. Tutuc, and M. Shayegan, Phys. Rev. B **79**, 195311 (2009).
[14] Y.-W. Tan, J. Zhu, H. L. Stormer, L. N. Pfeiffer, K. W. Baldwin, and K. W. West, Phys. Rev. Lett. **94**, 016405 (2005).
[15] R. P. Feynman and A. R. Hibbs, *Quantum Mechanics and Path Integrals* (McGraw-Hill, 1965).
[16] E. Y. Loh *et al.*, Phys. Rev. B **41**, 9301 (1990).
[17] J. Anderson, J. Chem. Phys. **69**, 1499 (1975).
[18] P. J. Reynolds, D. M. Ceperley, B. J. Alder, and W. A. Lester, J. Chem. Phys. **77**, 5593 (1982).
[19] M. Motta, D. E. Galli, S. Moroni, and E. Vitali, J. Chem. Phys. **140**, 024107 (2014).
[20] D. M. Ceperley, J. Stat. Phys. **63**, 1237 (1991).
[21] G. H. Booth, A. J. W. Thom, and A. Alavi, J. Chem. Phys. **131**, 054106 (2009).
[22] M. Feldbacher and F. F. Assaad, Phys. Rev. B **63**, 073105 (2001).
[23] D. M. Ceperley and B. Bernu, J. Chem. Phys. **89**, 6316 (1988); P.-M. Zimmerman, J. Toulouse, Z. Zhang, C.-B. Musgrave, and C.-J. Umrigar, *ibid.* **131**, 124103 (2009).
[24] M. Nava, A. Motta, D. E. Galli, E. Vitali, and S. Moroni, Phys. Rev. B **85**, 184401 (2012).
[25] G. H. Booth and G. Chan, J. Chem. Phys. **137**, 191102 (2012).
[26] G. H. Booth and G. Chan, Phys. Rev. B **91**, 155107 (2015).
[27] R. Blankenbecler, D. J. Scalapino, and R. L. Sugar, Phys. Rev. D **24**, 2278 (1981).
[28] G. Sugiyama and S. E. Koonin, Ann. Phys. **168**, 1 (1986).
[29] S. Zhang and H. Krakauer, Phys. Rev. Lett. **90**, 136401 (2003).
[30] S. Zhang, H. Krakauer, W. A. Al Saidi, and M. Suewettana, Comput. Phys. Commun. **169**, 394 (2005).
[31] S. Zhang, *Theoretical Methods for Strongly Correlated Electron Systems* (Springer-Verlag, 2003).
[32] S. Zhang, J. Carlson, and J. E. Gubernatis, Phys. Rev. B **55**, 7464 (1997).
[33] W. Purwanto and S. Zhang, Phys. Rev. E **70**, 056702 (2004).
[34] W. Purwanto, S. Zhang, and H. Krakauer, J. Chem. Phys. **130**, 094107 (2009).
[35] W. Purwanto, H. Krakauer, Y. Virgus, and S. Zhang, J. Chem. Phys. **135**, 164105 (2011).
[36] W. Purwanto, H. Krakauer, and S. Zhang, Phys. Rev. B **80**, 214116 (2009).
[37] K. Sawada, Phys. Rev. **106**, 372 (1957).
[38] S. Baroni and S. Moroni, Phys. Rev. Lett. **82**, 4745 (1999).
[39] J. Toulouse and C. J. Umrigar, J. Chem. Phys. **128**, 174101 (2008).
[40] M. Motta, G. Bertaina, D. E. Galli, and E. Vitali, Comput. Phys. Commun. **190**, 62–71 (2015).
[41] P. P. Ewald, Ann. Phys. **369**, 253 (1921).

[42]W. M. C. Foulkes, L. Mitas, R. J. Needs, and G. Rajagopal, Rev. Mod. Phys. **73**, 33 (2001).

[43]H. F. Trotter, Proc. Am. Math. Soc. **10**, 545 (1959).

[44]M. Suzuki, Prog. Theor. Phys. **56**, 1454 (1976).

[45]J. Hubbard, Phys. Rev. Lett. **3**, 77 (1959).

[46]R. L. Stratonovich, Sov. Phys. Doklady **2**, 416 (1957).

[47]A. M. Turing, Q. J. Mech. Appl. Math. **1**, 287 (1948).

[48]A. N. Tikhonov and V. Y. Arsenin, *Solution of Ill-posed Problems* (Winston & Sons, 1977).

[49]R. Balian and E. Brezin, Il Nuovo Cimento B **64**, 37 (1969).

[50]T. Gaskell, Proc. Phys. Soc. **77**, 1182 (1961); **80**, 1091 (1962).

[51]E. Vitali, M. Rossi, L. Reatto, and D. E. Galli, Phys. Rev. B **82**, 174510 (2010).

[52]K. Levenberg, Q. Appl. Math. **2**, 164 (1944); D. Marquardt, SIAM J. Appl. Math. **11**, 431 (1963).

[53]J. J. Shepherd, G. H. Booth, A. Grüneis, and A. Alavi, Phys. Rev. B **85**, 081103(R) (2012).

[54]J. J. Shepherd, G. H. Booth, and A. Alavi, J. Chem. Phys. **136**, 244101 (2012).

[55]H. Shi and S. Zhang, Phys. Rev. B **88**, 125132 (2013).

[56]F. Ma, W. Purwanto, S. Zhang, and H. Krakauer, Phys. Rev. Lett. **114**, 226401 (2015).

[57]E. Y. Loh, Jr., J. E. Gubernatis, R. T. Scalettar, R. L. Sugar, and S. R. White, *Interacting Electrons in Reduced Dimensions*, NATO ASI Series Vol. 213 (Plenum Press, 1989), pp. 55–60.

[58]C. N. Gilbreth and Y. Alhassid, Comput. Phys. Commun. **188**, 1–6 (2014).

[59]L. Fox, H. D. Huskey, and J. H. Wilkinson, Q. J. Mech. Appl. Math. **1**, 149 (1948).

[60]I. Tamm, J. Phys. (USSR) **9**, 499 (1945).

[61]S. M. Dancoff, Phys. Rev. **78**, 382 (1950).